CrossMark

CAMBRIDGE
UNIVERSITY PRESS

RESEARCH ARTICLE

Improved exponential weighted moving average based measurement noise estimation for strapdown inertial navigation system/doppler velocity log integrated system

Lanhua Hou, Xiaosu Xu,* Yiqing Yao, Di Wang, and Jinwu Tong

Key Laboratory of Micro-Inertial Instrument and Advanced Navigation Technology, Ministry of Education, School of Instrument Science and Engineering, Southeast University, Nanjing, China.
*Corresponding author. E-mail: xxs@seu.edu.cn

Abstract
The strapdown inertial navigation system (SINS) with integrated Doppler velocity log (DVL) is widely utilised in underwater navigation. In the complex underwater environment, however, the DVL information may be corrupted, and as a result the accuracy of the Kalman filter in the SINS/DVL integrated system degrades. To solve this, an adaptive Kalman filter (AKF) with measurement noise estimator to provide noise statistical characteristics is generally applied. However, existing methods like moving windows (MW) and exponential weighted moving average (EWMA) cannot adapt to a dynamic environment, which results in unsatisfactory noise estimation performance. Moreover, the forgetting factor has to be determined empirically. Therefore, this paper proposes an improved EWMA (IEWMA) method with adaptive forgetting factor for measurement noise estimation. First, the model for a SINS/DVL integrated system is established, then the MW and EWMA based measurement noise estimators are illustrated. Subsequently, the proposed IEWMA method which is adaptive to the various environments without experience is introduced. Finally, simulation and vehicle tests are conducted to evaluate the effectiveness of the proposed method. Results show that the proposed method outperforms the MW and EWMA methods in terms of measurement noise estimation and navigation accuracy.

1. Introduction

Research has shown that there are rich mineral resources in the ocean, which takes up three-quarters of the Earth's surface. The exploration of the vast ocean has become a momentous issue for humans. Underwater navigation technology, as the core technology of ocean exploration, is the most difficult challenge to tackle (Zhang et al., 2019). In the domain of underwater navigation, the strapdown inertial navigation system (SINS), with the performance characteristics of high autonomy and anti-interference, is widely utilised. But SINS has some performance deficiencies (e.g. unbounded position error growth and position/velocity/attitude Schuler oscillations). In light of this, acoustic positioning system, Doppler velocity log (DVL), Global Position System (GPS), depthmeter, and terrain matching are commonly introduced as alternatives to provide navigation information for underwater vehicles (González-García et al., 2020). Among these, DVL has become one of the main auxiliary navigation devices in underwater navigation by virtue of its reliability, autonomy and convenience. Recently, the SINS/DVL integrated system has developed into a reliable and important navigation system in underwater navigation (Yao et al., 2019).

The errors of the SINS/DVL integrated system can be categorised into inertial measurement unit (IMU) errors and DVL errors. The IMU is composed of three gyroscopes and three accelerometers to

provide angular velocity and specific force measurements (Sabet et al., 2018). The DVL is a device with four identical energy converters to output velocity information (Tal et al., 2017). Both are subject to scale factor, misalignment error, and random error. The fixed scale factor and misalignment error can be estimated in the calibration process. However, the random error of the IMU, sensitively influenced by temperature, pressure, and mechanical stresses, cannot be calculated in advance. To address this problem, a Kalman filter (KF) is introduced to estimate the random error of the IMU while blending the navigation information from the SINS and DVL (Narasimhappa et al., 2016, 2020; Eliav and Klein, 2018; Hu et al., 2018).

The optimality of KF relies on the correct prior knowledge of the process noise covariance matrix Q and the measurements noise covariance R (Mohamed and Schwarz, 1999). The matrix Q is often regarded as constant because the process noise in the navigation process is relatively invariable. Nevertheless, due to the complex underwater environment, such as ocean currents, marine organisms, changeable temperature and salinity, the random error of the DVL is variable and unpredicted. The affiliated matrix R is inconsistent with the reality and it will result in substantial estimation errors or even filter divergence. To solve this, two methods are proposed. One is the pure SINS method, which abandons the DVL information in cases where there is too much noise from the DVL. But then navigation errors accumulate quickly with time. The other is the adaptive KF (AKF) method, which estimates the statistical characteristics of the process and measurement noise to attenuate errors (Raman, 1972; Hu et al., 2020).

Since its inception, the use of AKF has become widespread in integrated navigation systems. Xu et al. researched the use of AKF in the USBL/INS integrated system (Xu et al., 2018). Liu et al. innovated an improved AKF for the INS/GPS integrated system of autonomous vehicles (Liu et al., 2018). Zhang et al. applied AKF to position correction based large depth navigation for autonomous underwater vehicles (AUV) (Zhang et al., 2020). This paper focuses on the application of AKF in the SINS/DVL integrated navigation system.

The AKF can be divided into four categories: Bayesian, maximum likelihood, correlation, and covariance matching. Each of them is based on the Bayes theorem and can be regarded as a particular form of Bayesian estimation. Based on the Bayesian estimation, a variational Bayesian based KF was proposed and successfully applied to INS/GPS integrated navigation (Huang and Zhang, 2017; Yulong et al., 2018). However, because of the high computational complexity, it is not widely used in underwater navigation. Based on the maximum likelihood principle, a novel adaptive unscented KF combining the maximum likelihood principle with moving horizon estimation was developed (Gao et al., 2017). The correlation method is based on the correlation of the output either directly or after a known linear operation. A correlation method based KF with nonlinear models was researched (Yang et al., 2018). To make the theoretical covariance consistent with the residual, covariance matching estimation is prevalent in integrated navigation systems by virtue of its simplicity of calculation and high accuracy (Jin et al., 2017).

As a covariance matching estimation strategy, the Sage–Husa AKF (SHAKF) was proposed and has become widely utilised (Sage and Husa, 1969; Liu et al., 2019). It estimates the real-time measurement noise covariance by the statistical information of historical epochs. According to the estimation theory, there are two kinds of measurement noise estimations: innovation adaptive estimation (IAE) and residual adaptive estimation (RAE) (Wang, 1999). In IAE the measurement noise is estimated by the average of innovations, in RAE it is calculated by the average of residuals. Almagbile et al. proved that with the same filter performance RAE is more reliable than IAE (Almagbile et al., 2010). To simplify computation and improve estimation accuracy, the moving windows (MW) method was proposed to estimate Q and R (Yang and Xu, 2003), and the exponential weighted moving average (EWMA) method was also introduced (Narasimhappa et al., 2018; Franzen and Fingscheidt, 2019; Xu et al., 2019). However, the optimal window width in MW and the forgetting factor in EWMA have to be determined empirically. Meanwhile, the fact that window width and forgetting factor cannot adapt to a dynamic environment results in unsatisfactory noise estimation performance.

Therefore, an improved EWMA (IEWMA) method for measurement noise estimation is proposed in this paper. An estimation convergence criterion based forgetting factor is improved to adapt to the
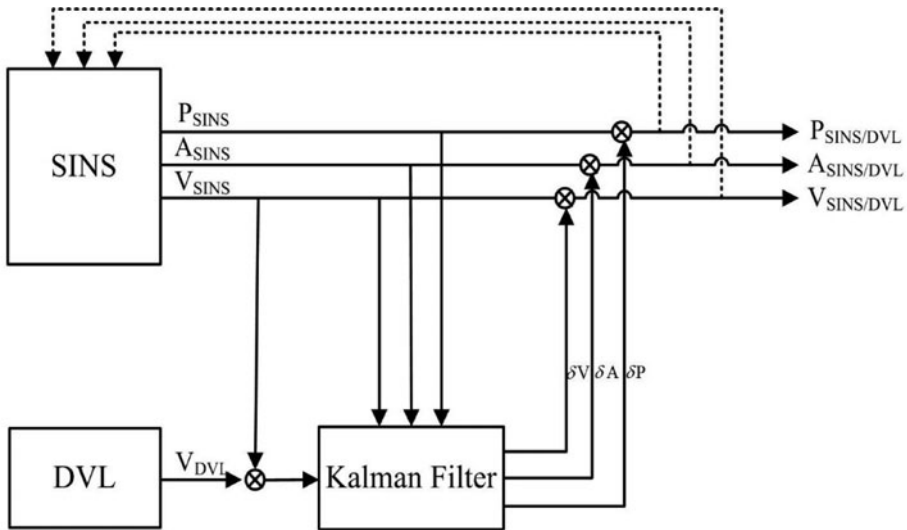
Figure 1. *Diagram of SINS/DVL integrated system.*

environment. Compared with the MW and EWMA methods, the IEWMA method can be applied to engineering practice without multiple experiences and the estimation results are more accurate.

The structure of this paper is as follows. In section 2, a SINS/DVL integrated system is designed. In section 3, the IAE and RAE based AKF methods are specifically illustrated, and MW, EWMA and the forgetting factor based IEWMA are presented. In section 4, the results of comprehensive simulation and vehicle tests conducted in this study are presented to illustrate the superiority of the proposed IEWMA method. Section 5 is devoted to the conclusion.

2. SINS/DVL integrated system

In the SINS/DVL integrated system, the loosely coupled method is frequently utilised. This is because the information provided by DVL is generally the velocity information rather than the original information of the four acoustic channels. The diagram of the SINS/DVL integrated system is shown in Figure 1. The KF fuses the navigation information from the SINS with the velocity from the DVL and then updates the navigation errors to correct the navigation results. In addition, the gyroscope errors, accelerometer errors, and DVL scale factor can also be estimated as a part of the state vector. To cast the integrated process in the KF framework, the state equation and measurement equation are established by the time rate differential equations of SINS and the velocity difference of SINS and DVL in the body frame.

2.1. State equation

The state equation is established as follows:

$$X' = FX + GW \tag{2.1}$$

where X is the state vector, F is the state transition matrix, G is the system noise matrix and W is the process noise vector. The state vector X is defined as (Hu et al., 2019):

$$X = \begin{bmatrix} \phi_x & \phi_y & \phi_z & \delta V_E^n & \delta V_N^n & \delta V_U^n & \delta\lambda & \delta L & \delta h & \varepsilon_x \\ \varepsilon_y & \varepsilon_z & \nabla_x & \nabla_y & \nabla_z & K_d \end{bmatrix}^T \tag{2.2}$$

where K_d is the DVL scale factor, and the matrix $\boldsymbol{F}$, $\boldsymbol{G}$, and $\boldsymbol{W}$ are expressed as follows:

$$\boldsymbol{F} = \begin{bmatrix} \boldsymbol{F}_{aa} & \boldsymbol{F}_{av} & \boldsymbol{F}_{ap} & -\boldsymbol{C}_b^n & \boldsymbol{0}_{3\times3} & \\ \boldsymbol{F}_{va} & \boldsymbol{F}_{vv} & \boldsymbol{F}_{vp} & \boldsymbol{0}_{3\times3} & \boldsymbol{C}_b^n & \boldsymbol{0}_{9\times1} \\ \boldsymbol{0}_{3\times3} & \boldsymbol{F}_{pv} & \boldsymbol{F}_{pp} & \boldsymbol{C}_b^n & \boldsymbol{0}_{3\times3} & \\ & & \boldsymbol{0}_{7\times15} & & & \end{bmatrix}, \; \boldsymbol{G} = \begin{bmatrix} -\boldsymbol{C}_b^n & \boldsymbol{0}_{3\times3} \\ \boldsymbol{0}_{3\times3} & \boldsymbol{C}_b^n \\ \boldsymbol{0}_{10\times3} & \boldsymbol{0}_{10\times3} \end{bmatrix}, \; \boldsymbol{W} = \begin{bmatrix} \boldsymbol{w}_g^b \\ \boldsymbol{w}_a^b \end{bmatrix} \quad (2.3)$$

where $\boldsymbol{F}_{aa}, \boldsymbol{F}_{av}, \boldsymbol{F}_{ap}, \boldsymbol{F}_{va}, \boldsymbol{F}_{pv}, \boldsymbol{F}_{vv}, \boldsymbol{F}_{pp}, \boldsymbol{F}_{vp}$ are determined by the error equation of SINS, $\boldsymbol{C}_b^n$ is the transfer matrix from frame b to frame n, and $\boldsymbol{w}_g^b$ and $\boldsymbol{w}_a^b$ are the error of gyroscope and accelerometer, respectively.

2.2. Measurement equation

The measurement equation is modelled as follows (Lee et al., 2005):

$$\boldsymbol{Z} = \hat{\boldsymbol{V}}_b - \boldsymbol{V}_{bDVL} = \boldsymbol{H}\boldsymbol{X} + \boldsymbol{V} \quad (2.4)$$

where $\boldsymbol{Z}$ is the measured matrix, $\hat{\boldsymbol{V}}_b$ is the velocity calculated by SINS in the body frame, $\boldsymbol{V}_{bDVL}$ is the velocity provided by DVL, $\boldsymbol{H}$ is the measurement transfer matrix and $\boldsymbol{V}$ is the measurement information noise. The measurement transfer matrix is:

$$\boldsymbol{H} = \begin{bmatrix} \boldsymbol{C}_{31}V_N - \boldsymbol{C}_{21}V_U & \boldsymbol{C}_{11}V_U - \boldsymbol{C}_{31}V_E & \boldsymbol{C}_{21}V_E - \boldsymbol{C}_{11}V_N & & & -V_{x\_bDVL} \\ \boldsymbol{C}_{32}V_N - \boldsymbol{C}_{22}V_U & \boldsymbol{C}_{12}V_U - \boldsymbol{C}_{32}V_E & \boldsymbol{C}_{22}V_E - \boldsymbol{C}_{12}V_N & \boldsymbol{C}_n^b & \boldsymbol{0}_{3\times9} & -V_{y\_bDVL} \\ \boldsymbol{C}_{33}V_N - \boldsymbol{C}_{23}V_U & \boldsymbol{C}_{13}V_U - \boldsymbol{C}_{33}V_E & \boldsymbol{C}_{23}V_E - \boldsymbol{C}_{13}V_N & & & -V_{z\_bDVL} \end{bmatrix} \quad (2.5)$$

3. AKF

Theoretically, the success of the SINS/DVL integrated navigation system strongly depends on the precision of the measurement noise estimation. In this sense, IAE and RAE are proposed for measurement noise estimation by the average of the innovations and residuals over all epochs. However, the historical statistical information may lead to sluggish and biased noise estimation. To solve this problem, two methods are commonly employed. The MW method calculates the average of the innovation or residual information nearing the current epoch in the moving window. The EWMA method calculates the exponential weighted average of the innovation or residual information. However, inappropriate window width of MW and the forgetting factor of EWMA in the dynamic environment may result in undesirable navigation errors. The optimal window width and the forgetting factor have to be determined empirically. Hence, a more reliable method remains to be elucidated. To best of our knowledge, the fixed forgetting factor in EWMA represents the oblivion speed of the historical sequence. In order to improve the noise estimation accuracy, the oblivion speed needs to be adapted to the underwater environment. Therefore, an adaptive forgetting factor based IEWMA method for measurement noise estimation in the INS/DVL integrated system is proposed in this paper.

3.1. AKF with noise measurement estimator based on IAE and RAE

First, the dynamic system is modelled as:

$$\begin{cases} \boldsymbol{X}_k = \boldsymbol{\Phi}_{k,k-1}\boldsymbol{X}_{k-1} + \boldsymbol{\Gamma}_{k-1}\boldsymbol{W}_{k-1} \\ \boldsymbol{Z}_k = \boldsymbol{H}_k\boldsymbol{X}_k + \boldsymbol{V}_k \end{cases} \quad (3.1)$$

where $\boldsymbol{X}_k$ is the state vector, $\boldsymbol{\Phi}_{k,k-1}$ is the one-step transfer matrix from epoch k-1 to k, $\boldsymbol{\Gamma}_{k-1}$ is the system noise matrix, $\boldsymbol{W}_{k-1}$ is the system noise, $\boldsymbol{Z}_k$ is the measurement vector, $\boldsymbol{H}_k$ is the measurement

matrix, and V_k is the measurement noise. W_{k-1} and V_k are supposed to be uncorrelated zero-mean Gaussian white noise sequences with the statistical characteristics:

$$\begin{cases} E[W_k] = q_k, Cov[W_k, W_j] = Q_k \delta_{kj} \\ E[V_k] = r_k, Cov[V_k, V_j] = R_k \delta_{kj} \\ Cov[W_k, V_j] = 0 \end{cases} \tag{3.2}$$

where q_k is the mean of the process noise, Q_k is the covariance of the process noise, r_k is the mean of the measurement noise, R_k is the covariance of the measurement noise and δ_{kj} is the Kronecker data function. The conventional KF is described as follows:

$$X_{k,k-1} = \mathbf{\Phi}_{k-1} \hat{X}_{k-1} \tag{3.3}$$

$$P_{k,k-1} = \mathbf{\Phi}_{k-1} P_{k-1} \mathbf{\Phi}_{k-1}^T + \mathbf{\Gamma}_{k-1} Q_{k-1} \mathbf{\Gamma}_{k-1}^T \tag{3.4}$$

$$K_k = P_{k,k-1} \mathbf{H}_k^T (\mathbf{H}_k P_{k,k-1} \mathbf{H}_k^T + R_k)^{-1} \tag{3.5}$$

$$\hat{X}_k = \hat{X}_{k,k-1} + K_k (\mathbf{Z}_k - H_k \hat{X}_{k,k-1}) \tag{3.6}$$

$$P_k = (I - K_k H_k) P_{k,k-1} \tag{3.7}$$

where $X_{k,k-1}$ is the predicted state estimate, $P_{k,k-1}$ is the predicted estimate covariance, P_k is the updated estimate covariance and K_k is the Kalman gain matrix.

3.1.1. AKF with noise measurement estimator based on IAE

An AKF with measurement noise estimator based on IAE can be driven as follows:

Defining the innovation as:

$$\varepsilon_k = \mathbf{Z}_k - H_k \hat{X}_{k,k-1} \tag{3.8}$$

Using Equation (3.1), it can be directly driven that,

$$\varepsilon_k = H_k X_k + v_k - H_k \hat{X}_{k,k-1} = H_k (X_k - \hat{X}_{k,k-1}) + v_k \tag{3.9}$$

Calculating the covariance of innovation:

$$\begin{aligned} E(\varepsilon_k \varepsilon_k^T) &= E\left\{ \left\{ H_k (X_k - \hat{X}_{k,k-1}) + v_k \right\} \left\{ H_k \left(X_k - \hat{X}_{k,k-1} \right) + v_k \right\}^T \right\} \\ &= E\left\{ H_k \left(X_k - \hat{X}_{k,k-1} \right) \left(X_k - \hat{X}_{k,k-1} \right)^T H_k^T + v_k v_k^T \right\} \\ &= E\left\{ H_k \left(X_k - \hat{X}_{k,k-1} \right) \left(X_k - \hat{X}_{k,k-1} \right)^T H_k^T \right\} + E\{ v_k v_k^T \} \\ &= H_k P_{k,k-1} H_k^T + R_k \end{aligned} \tag{3.10}$$

Accordingly, the covariance of measurement noise can be described as:

$$R_k = E(\varepsilon_k \varepsilon_k^T) - H_k P_{k,k-1} H_k^T = \frac{1}{k} \sum_{i=1}^{k} \left\{ \varepsilon_i \varepsilon_i^T \right\} - H_k P_{k,k-1} H_k^T \tag{3.11}$$

3.1.2. AKF with noise measurement estimator based on RAE

An AKF with measurement noise estimator based on RAE can be driven as follows:

Defining the residual as:

$$\gamma_k = \mathbf{Z}_k - H_k \hat{X}_k \tag{3.12}$$

Using Equations (3.6) and (3.8), it can be directly obtained that,

$$\boldsymbol{\gamma}_k = \boldsymbol{Z}_k - \boldsymbol{H}_k(\widehat{\boldsymbol{X}}_{k,k-1} + \boldsymbol{K}_k\boldsymbol{\varepsilon}_k) = \boldsymbol{Z}_k - \boldsymbol{H}_k\widehat{\boldsymbol{X}}_{k,k-1} - \boldsymbol{H}_k\boldsymbol{K}_k\boldsymbol{\varepsilon}_k = (\boldsymbol{I} - \boldsymbol{H}_k\boldsymbol{K}_k)\boldsymbol{\varepsilon}_k \tag{3.13}$$

Calculating the covariance of residual by the error propagation law (Wang, 1999):

$$E(\gamma_k{\gamma_k}^T) = R_k - H_kP_kH_k^T \tag{3.14}$$

Accordingly, the covariance of measurement noise can be described as:

$$R_k = E(\gamma_k{\gamma_k}^T) + H_kP_kH_k^T = \frac{1}{k}\sum_{i=1}^{k}\left\{\gamma_i{\gamma_i}^T\right\} + H_kP_kH_k^T \tag{3.15}$$

By the way, Equation (3.15) can also be obtained via maximum likelihood criterion (Mohamed and Schwarz, 1999). Comparing the two methods, subtraction in the IAE method inevitably results in negative definite R_k and then leads the filter to diverge. For this reason, the RAE method is more reliable and powerful in practical application. The measurement noise estimator in this paper is based on the RAE method.

3.2. AKF based on measurement noise estimator

It is noted that the measurement noise estimator based on IAE or RAE calculates R_k by the average of the innovations or residuals over all epochs. The average of the historical information may result in estimation latency. For example, when the measurement noise occurs in the hundredth epoch, the influence of the residual in the hundredth epoch to the system is merely 1% as the same as the epoch 1 to 99. The residuals which approach zero at the epoch 1 to 99 lead to sluggish and biased measurement noise estimation. From this point of view, it is necessary to reduce the weight of the historical epochs. Therefore, MW and EWMA are introduced.

The MW method employs a moving window to store the residuals and calculates the average of them for R_k. The EWMA method averages the residuals over all epochs with the exponential weight. The principles of the two methods are shown in Figure 2. The colour depth represents the average weight of the residual. The darker the colour, the greater the weight. It can be seen that R_k in the MW method is the average of the residuals in the moving window and in the EWMA method the closer to the current epoch, the greater the weight.

3.2.1. Measurement noise estimator based on MW
The MW method estimates the measurement noise matrix through computing the average of the residuals in a moving window, which effectively eliminates the influence of the historical information. The general equation of MW is:

$$\hat{\boldsymbol{R}}_k = \frac{1}{m}\sum_{i=k-m+1}^{k}\left\{\boldsymbol{\gamma}_i\boldsymbol{\gamma}_i^T + \boldsymbol{H}_i\boldsymbol{P}_i\boldsymbol{H}_i^T\right\} \tag{3.16}$$

where m is the width of the moving window, and k is the current epoch.

To enhance the operation efficiency, Equation (3.16) can be expressed as:

$$\hat{\boldsymbol{R}}_k = \hat{\boldsymbol{R}}_{k-1} + \frac{1}{m}\left\{\left(\boldsymbol{\gamma}_k\boldsymbol{\gamma}_k^T + \boldsymbol{H}_k\boldsymbol{P}_k\boldsymbol{H}_k^T\right) - \left(\boldsymbol{\gamma}_{k-m}\boldsymbol{\gamma}_{k-m}^T + \boldsymbol{H}_{k-m}\boldsymbol{P}_{k-m}\boldsymbol{H}_{k-m}^T\right)\right\} \tag{3.17}$$

The optimal width of the moving window is determined by the dynamic characteristic of the environment. In highly dynamic circumstances, the width of the moving window is required to be small to detect changes sensitively. Conversely, in low dynamic circumstances, the width of the moving window is required to be great to improve the stability of the system.
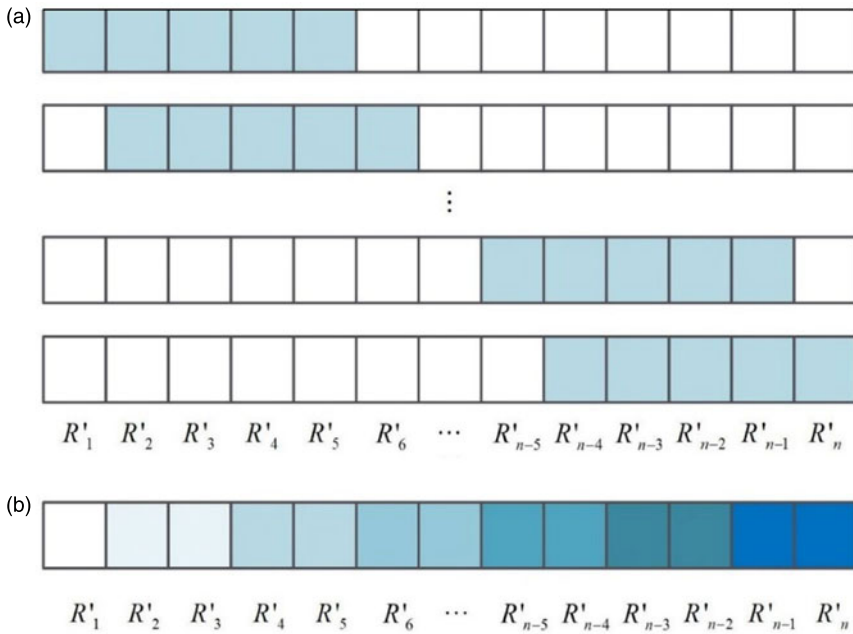
Figure 2. *(a) Diagram of MW method. (b) Diagram of EWMA method.*

3.2.2. Measurement noise estimator based on EWMA

R_k of the EWMA method is estimated with the exponential weighted average of the residuals over all epochs. The closer to the current epoch, the greater the weight. It effectively reduces the undesirable influence of the historical sequence. The general equation of EWMA is (Sun et al., 2016; Narasimhappa et al., 2018):

$$\hat{\boldsymbol{R}}_k = (1 - d_k)\hat{\boldsymbol{R}}_{k-1} + d_k(\boldsymbol{\gamma}_k\boldsymbol{\gamma}_k^T + \boldsymbol{H}_k\boldsymbol{P}_k\boldsymbol{H}_k^T)$$
$$d_k = \frac{1 - b}{1 - b^{k+1}} \tag{3.18}$$

where k is the time step, d_k is the forgetting factor, b is a constant, $b \in (0 \cdot 9, 1]$.

It can be seen that the EWMA method estimates R_k by the residual of the current epoch and the calculated R_{k-1} of the previous epoch. Without the space to store the residuals of historical epochs and complex computing, EWMA is more applicable to implementation. The principle of EWMA is illustrated as follows:

To calculate the measurement noise covariance matrix R_k in the k-th epoch with the exponential weighted average of the residuals over the whole historical epochs, the recursive formula is given:

$$\hat{\boldsymbol{R}}_k = (1 - d)\hat{\boldsymbol{R}}_{k-1} + d\hat{\boldsymbol{R}}_k' \tag{3.19}$$

where $\hat{\boldsymbol{R}}_k' = \boldsymbol{\gamma}_k\boldsymbol{\gamma}_k^T + \boldsymbol{H}_k\boldsymbol{P}_k\boldsymbol{H}_k^T$.

With the recursive formula, $\hat{\boldsymbol{R}}_k$ can be expanded as:

$$\begin{aligned}
\hat{\boldsymbol{R}}_1 &= (1 - d)\hat{\boldsymbol{R}}_0 + d\hat{\boldsymbol{R}}_1' \\
\hat{\boldsymbol{R}}_2 &= (1 - d)\hat{\boldsymbol{R}}_1 + d\hat{\boldsymbol{R}}_2' = (1 - d)^2\hat{\boldsymbol{R}}_0 + (1 - d)d\hat{\boldsymbol{R}}_1' + d\hat{\boldsymbol{R}}_2' \\
\hat{\boldsymbol{R}}_3 &= (1 - d)\hat{\boldsymbol{R}}_2 + d\hat{\boldsymbol{R}}_3' = (1 - d)^3\hat{\boldsymbol{R}}_0 + (1 - d)^2d\hat{\boldsymbol{R}}_1' + (1 - d)d\hat{\boldsymbol{R}}_2' + d\hat{\boldsymbol{R}}_3' \\
&\cdots \\
\hat{\boldsymbol{R}}_k &= (1 - d)\hat{\boldsymbol{R}}_{k-1} + d\hat{\boldsymbol{R}}_k' = (1 - d)^k\hat{\boldsymbol{R}}_0 + (1 - d)^{k-1}d\hat{\boldsymbol{R}}_1' + (1 - d)^{k-2}d\hat{\boldsymbol{R}}_2' + \cdots + d\hat{\boldsymbol{R}}_k'
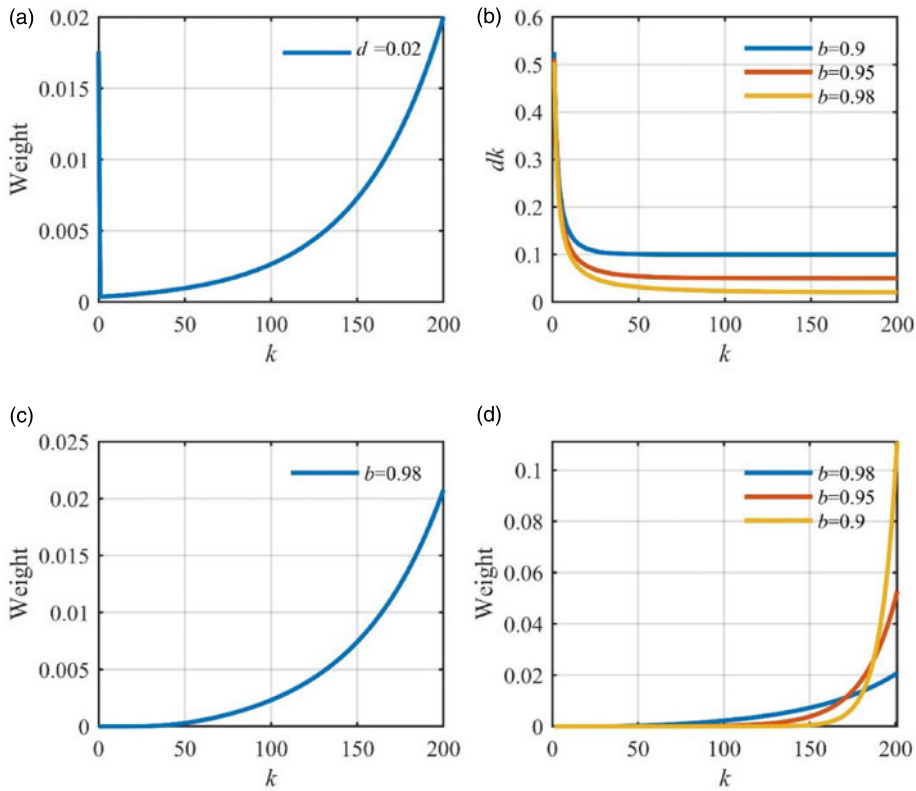\end{aligned} \tag{3.20}$$

Figure 3. *(a) Weight in each epoch before bias correction. (b) d_k in bias correction. (c) Weight in each epoch after bias correction. (d) Relation between weight in each epoch and b..*

where $\hat{R}_0$ is set from experience and d is the forgetting factor, $d \in (0, 0 \cdot 1]$. It can be seen in the last equation of Equation (3.20) that R_k is the exponential weighted average over the historical epochs. Regretably, the multiplier d for the exponential item is missed in the first coefficient. For clarity, the weight of historical epoch in the 200th epoch ($k = 200$) is shown in Figure 3(a). It can be seen that the weight increases exponentially, but there is a conspicuous bias in the initial epoch. Consequently, the weight of the initial epoch is bigger than others. To address this problem, bias correction is introduced:

$$d_k = \frac{1-b}{1-b^{k+1}}, \quad b \in [0.9, 1) \tag{3.21}$$

The value of d_k is shown in Figure 3(b). As k increases, d_k decreases from a large value to $1-b$. When $k = 1$, $1/d_k$ is a small value. In consequence, the weight of the first epoch is reduced and the bias is corrected. The weight of each epoch with bias correction is shown in Figure 3(c). Compared with Figure 3(a), the bias is distinctly corrected.

Different b represents the different average performance. Figure 3(d) shows the relation of weight and b. It can be seen that the smaller b, the bigger the weight of the current epoch and the smaller the weight of the historical epochs. In highly dynamic circumstances, b is required to decrease to immediately detect changes. Conversely, in low dynamic circumstances, b is required to increase to improve the stability of the system. Therefore, an improved EWMA based on the adaptive b is proposed in the next section.
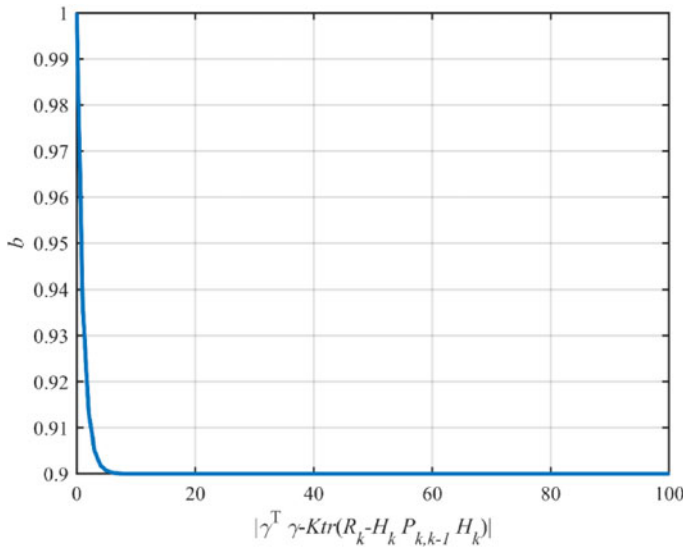
Figure 4. *Relation between b and the exponential term.*

3.2.3. Measurement noise estimator based on IEWMA

In order to estimate the variable measurement noises in different dynamic environments and improve navigation accuracy, the measurement noise estimator based on IEWMA with adaptive forgetting factor is proposed in this paper.

Conceptually, the discrepancy between the residual covariance estimation and the theoretical residual covariance can be employed to evaluate the stability of the measurement noise estimator (Gao et al., 2015). The estimation convergence criterion can be represented as:

$$\left| \boldsymbol{\gamma}^T \boldsymbol{\gamma} - \kappa tr(\hat{R}_k - H_k P_{k,k-1} H_k^T) \right| \begin{cases} > 0 & \text{unstable} \\ = 0 & \text{stable} \end{cases} \tag{3.22}$$

Where κ is constant and determined by the empirical knowledge.

According to the analysis in section 3.2, when the measurement noise is stable, the forgetting factor b is required to be large, whereas when the measurement noise is unstable, the forgetting factor b is required to be small. When $b = 0.9$, R_k is approximately the average over the 10 epochs before the current epoch. When $b = 0.98$, R_k is approximately the average over the 50 epochs, and it is the average over the whole epochs when b approaches 1. Empirically, it is appropriate to calculate R_k according to the average over 10 more epochs. Therefore, $b \in [0.9, 1)$ is supposed in the paper. Accordingly, in this paper the adaptive b is defined as:

$$b = 0.9 + 0.1 e^{-|\boldsymbol{\gamma}^T \boldsymbol{\gamma} - \kappa tr(\hat{R}_k - H_k P_{k,k-1} H_k^T)|} \tag{3.23}$$

where κ is constant and $\kappa = 5$.

Figure 4 shows the relation between b and the exponential term. It can be seen that, with the increasing exponential term, the value of b increases from 0·9 to 1. In high dynamic circumstances, the exponential term is large and b approaches 0·9. Conversely, in low dynamic circumstances, the exponential term goes to zero and b approaches 1.

The superiority of the AKF based on IEWMA with the adaptive forgetting factor is listed as follows:

1. It is adaptable for various dynamic characteristics.
2. It can be applied to engineering practice without multiple experiences.
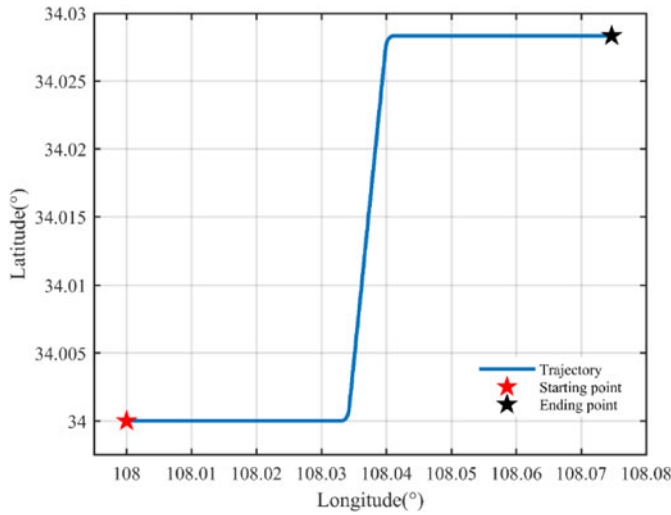
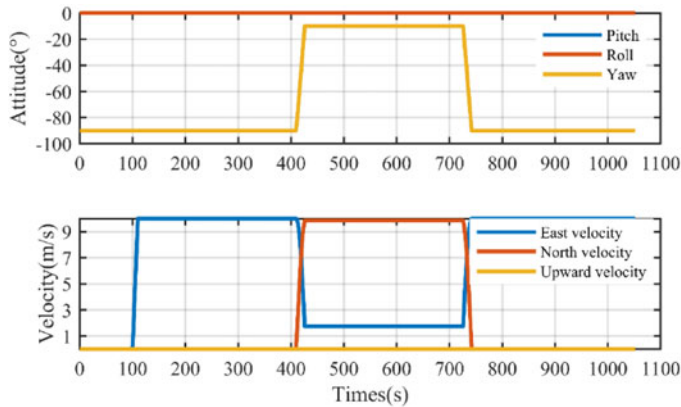**Figure 5.** *Trajectory of the vehicle in simulation.*

Figure 6. *Dynamic characteristics of vehicle in simulation.*

3. The estimation result is more stable in low dynamic circumstances and more sensitive in highly dynamic circumstances.

4. Simulation and vehicle tests

The performances of the SINS/DVL integrated system based on AFK with measurement noise estimator of MW, EWMA and IEWMA are evaluated on simulation and vehicle tests.

4.1. Simulation

A trajectory lasting for about 1,000 s with three straight lines and two curves is simulated. The simulated trajectory and vehicle dynamic characteristics are shown in Figures 5 and 6. The start point is set as latitude 34° N and longitude 108° E. The initial attitude is set as [0°, 0°, −90°]. The initial attitude error is set as [0·1°, 0·1°, 0·5°]. The drift bias and the random walk noise of the accelerometer are set as 50 μg and 50 μg/$\sqrt{\text{Hz}}$, and those of the gyroscope are set as 0.01°/$\sqrt{h}$ and 0.01°/$\sqrt{h}$. The DVL scale factor is set as 0·005. The update rates of the IMU and DVL are set as 200 Hz and 1 Hz, respectively.
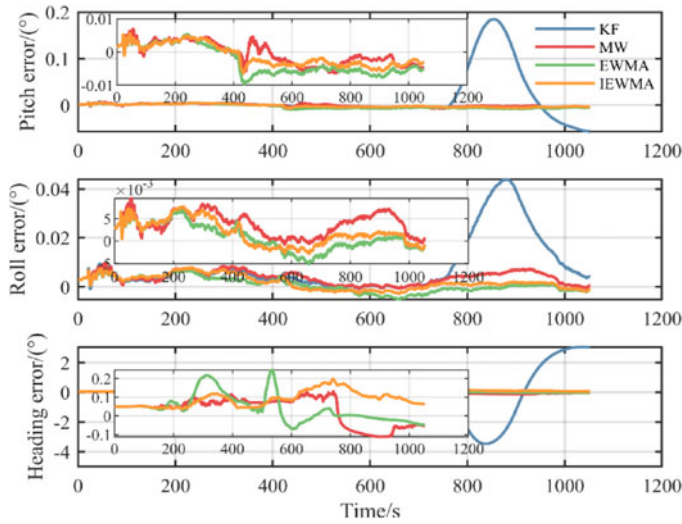
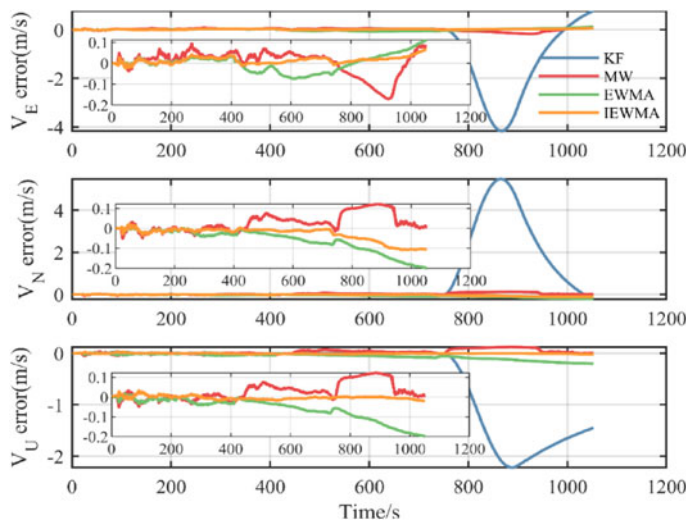**Figure 7.** *Attitude errors of four methods in simulation.*

Figure 8. *Velocity errors of four methods in simulation.*

In order to compare the performances of these methods, it is simulated that a graded noise with the sine function of 5 m/s occurs from 750 s to 900 s whereas the noise at other times is zero-mean white noise with standard deviation of 0·1 m/s. Fairly, the optimal window length was found to be 50, and the forgetting factor $b = 0·97$ after quite a few experiments to compare with the proposed method. Meanwhile, the conventional KF was also carried out to emphasise the performance of the proposed method. The comparisons of attitude, velocity and position errors of the four algorithms are shown in Figures 7–9, where the blue line, red line, green line and orange line represent KF, MW, EWMA and IEWMA, respectively. When noise occurs, the conventional KF immediately diverges. Conversely, with the measurement noise estimator, other methods are relatively stable. Looking at the enlarged drawing, we can find that the errors of IEWMA method are more stable and smaller than the others.

In order to compare intuitively the performances of the four methods, the horizontal position errors of KF and AKF with the measurement noise estimators of MW, EWMA and IEWMA are shown in
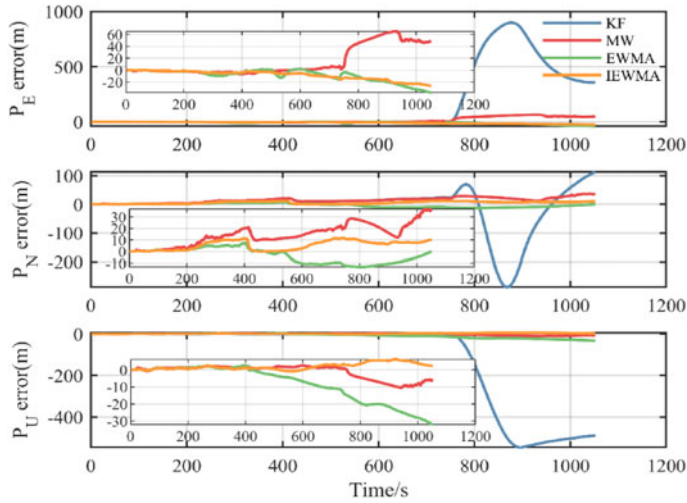
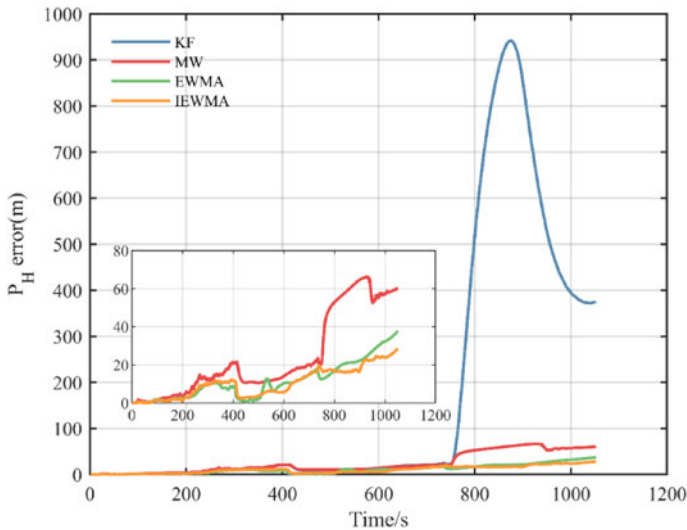**Figure 9.** *Position errors of four methods in simulation.*

Figure 10. *Horizontal position errors of four methods in simulation.*

Figure 10. It can be seen that the horizontal position error of IEWMA is more stable and smaller than the others.

Quantitative analysis was carried out on the navigation errors via the mean representing the size of the errors and the root mean square (RMS) representing the stability of the errors. The mean and RMS of the attitude, velocity and position errors are shown in Tables 1 and 2, respectively. The mean and RMS of horizontal position errors in the four methods are shown in Table 3.

From Table 1, we can see that the mean of velocity and position errors in IEWMA is smaller than the others. The differences of attitude error in MW, EWMA and IEWMA are negligible. Meanwhile, the RMS of all errors in the IEWMA method is smaller than the others in Table 2. It is also obvious that the mean and RMS of horizontal position error in IEWMA are smaller than the others in Table 3. Therefore, it is concluded that IEWMA outperforms MW and EWMA in both navigation accuracy and stability.

As mentioned, performance of the integrated system depends on the accuracy of the estimated R_k. The estimated R_k is shown in Figure 11. As anticipated, R_k of IEWMA is the nearest to the true value.

Table 1. *Mean of attitude, velocity and position errors in four methods.*

Method	Attitude (pitch)	Attitude (roll)	Attitude (yaw)	Velocity (E)	Velocity (N)	Velocity (U)	Position (E)	Position (N)	Position (U)
KF	0·02334	0·008384	0·680781	0·490694	0·71575	0·43585	159·2005	37·31923	115·0909
MW	3·09E-03	3·84E-03	0·075191	0·046104	0·037349	0·016047	16·42181	14·48248	9·074417
EWMA	4·55E-03	2·49E-03	0·058677	0·0322	0·060196	0·045957	8·879652	5·618469	2·983621
IEWMA	3·23E-03	2·41E-03	0·058535	0·016455	0·029387	0·007298	8·319802	5·427956	2·037195

Table 2. *RMS of attitude, velocity and position errors in four methods.*

Method	Attitude (pitch)	Attitude (roll)	Attitude (yaw)	Velocity (E)	Velocity (N)	Velocity (U)	Position (E)	Position (N)	Position (U)
KF	5·08E-02	1·40E-02	1·300867	1·156426	1·653638	0·875787	321·2462	72·78223	234·7398
MW	3·42E-03	4·56E-03	7·87E-02	0·058616	0·052076	0·022114	27·70016	17·11626	13·28029
EWMA	5·00E-03	3·05E-03	8·20E-02	0·040637	0·081803	0·058244	13·20689	7·145725	4·160389
IEWMA	3·41E-03	3·02E-03	7·84E-02	0·021147	0·044574	9·19E-03	11·11109	6·773047	2·706211

Table 3. Mean and RMS of horizontal position errors in four methods.

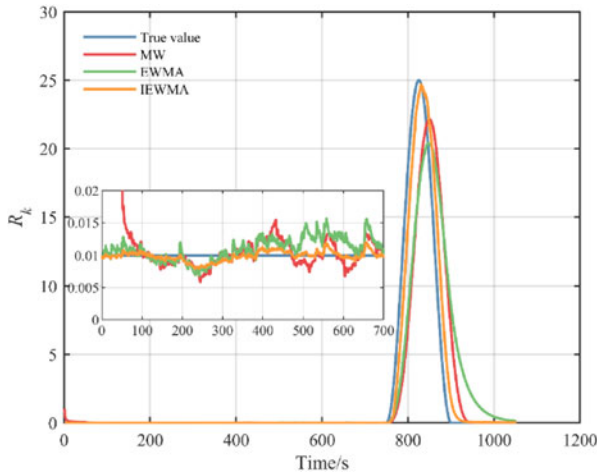| Method	KF	MW	EWMA	IEWMA
Mean	169·1027	24·12699	11·36973	10·39009
RMS	329·3879	32·56171	15·0161	13·01271

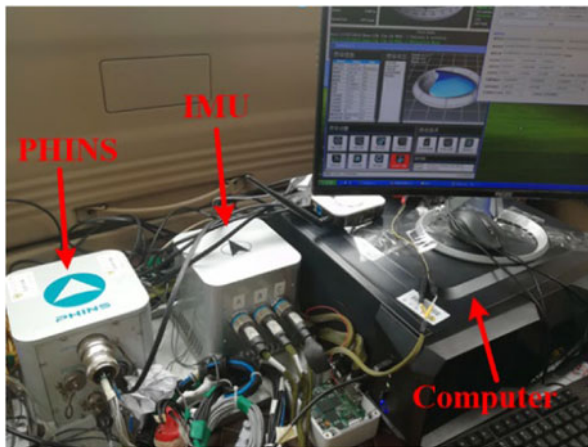*Figure 11. Diagram of estimated R_k in simulation.*

Figure 12. Installation structure for land trial.

On the one hand, R_k of IEWMA is more stable than the others in 0 s to 600 s. This is because, in cases where the measurement noise is stable, adaptive forgetting factor b becomes as small as possible. Accordingly, the weight of the current epoch decreases and the weight of historical sequence increases. On the other hand, R_k of IEWMA is more susceptible than others in 750 s to 900 s. Similarly, when noise occurs, adaptive forgetting factor b becomes as large as possible. Accordingly, the weight of the current epoch increases and the weight of the historical sequence decreases. The undesirable influence of historical sequence in IEWMA is eliminated. However, R_k of MW and EWMA is still influenced by the historical sequence and it is hysteretic to the volatile noise.
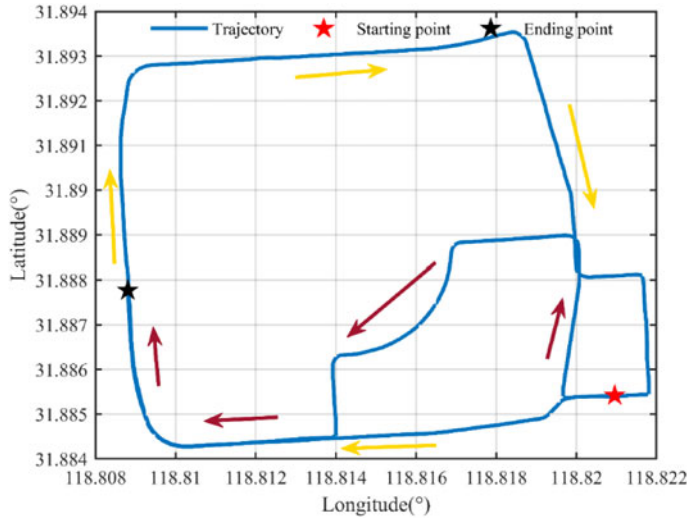
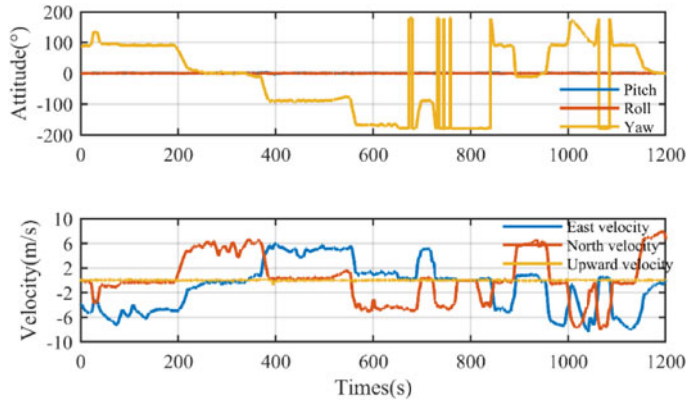**Figure 13.** *Trajectory of the vehicle in land trial.*

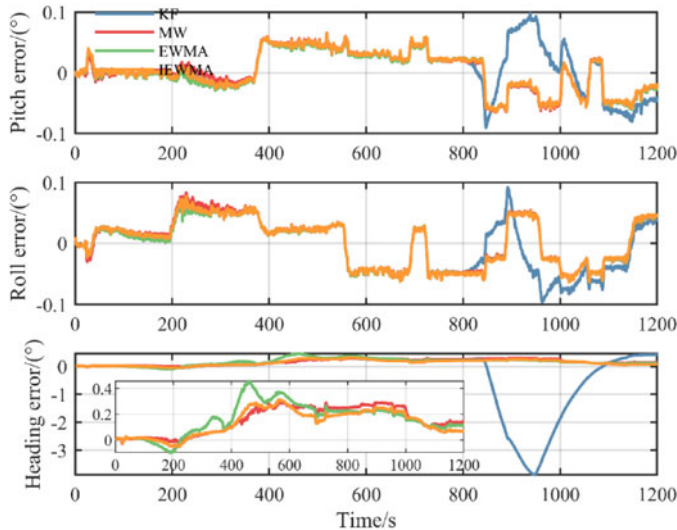**Figure 14.** *Dynamic characteristics of vehicle in land trial.*

Figure 15. *Attitude errors of four methods in land trial.*

Table 4. *Specifications of IMU and PHINS.*

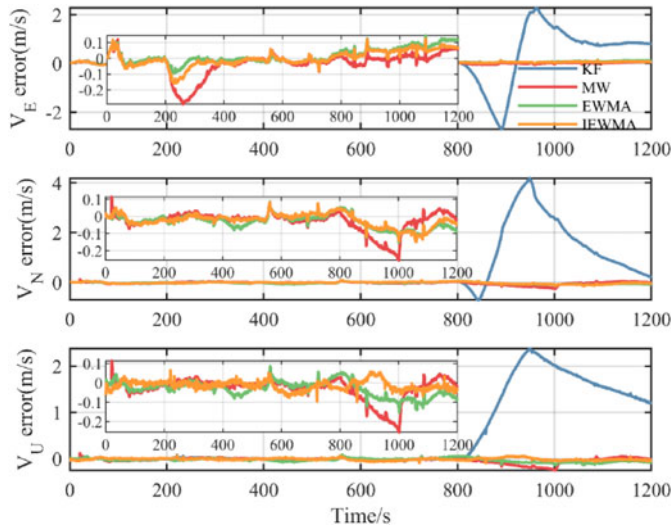| Sensor	Parameter	Accuracy	Rate
IMU	Gyroscope bias stability	$\leq 0.02°/h$	200 Hz
	Gyroscope random walk	$\leq 0.005°/\sqrt{h}$	200 Hz
	Accelerometer bias variation	$\pm 50\,\mu g$	200 Hz
	Accelerometer output noise	$\leq 50\,\mu g/\sqrt{Hz}$	200 Hz
PHINS	Attitude (GPS aided mode)	$\leq 0.01°$	200 Hz

Figure 16. *Velocity errors of four methods in land trial.*

4.2. Vehicle test

The proposed method was evaluated in land vehicle field testing to predict the feasibility of its operation in underwater environments. In the SINS/DVL navigation system used in the vehicle test, the inertial information is provided by the IMU and the velocity information of DVL is replaced by the PHINS which is developed by French firm IXBLU. PHINS transforms its own velocity from navigation frame to body frame using the true attitude information to provide the DVL information. A computer was utilised to perform a series of navigation operations. The installation structure is shown in Figure 12. The specifications of the IMU and PHINS are listed in Table 4.

The land trial was conducted near 31° 88′N, 118° 82′E, on the campus of Southeast University. The vehicle trajectory, lasting for 1,200 s, is shown in Figure 13 and vehicle dynamic characters are shown in Figure 14.

In the vehicle test, the graded noise with the sine function of 5 m/s is contrived from 800 s to 950 s to compare the performances of these methods. Fairly, the optimal width of the moving window for MW is set as 50 and the optimal forgetting factor *b* for EWMA is set as 0·98 after multiple experiences. The attitude, velocity and position errors of the four methods are shown in Figures 15–17. Meanwhile, horizontal position errors are shown in Figure 18. Similarly, the errors of the IEWMA method are the most stable and lowest in the four methods, which effectively verifies the feasibility of the proposed method.

Simultaneously, quantitative analysis is performed. The mean and RMS of attitude, velocity, individual position and horizontal position errors are shown in Tables 5–7. From Tables 5 and 6, we can see that the mean and RMS of errors for IEWMA is smaller than for KF, MW and EWMA. In Table 7, it
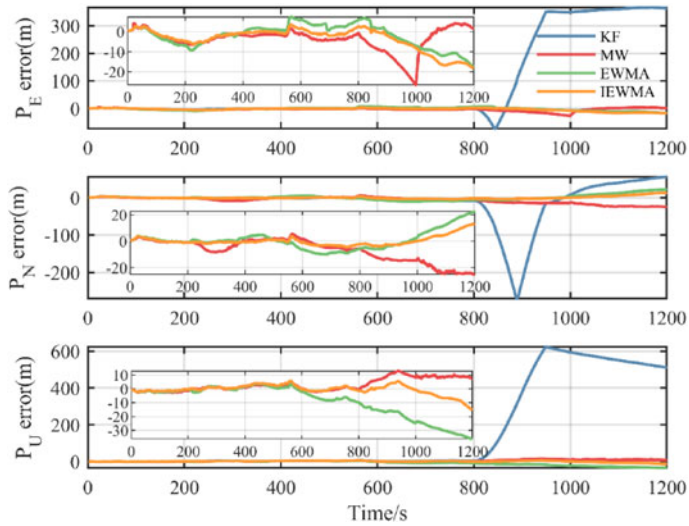
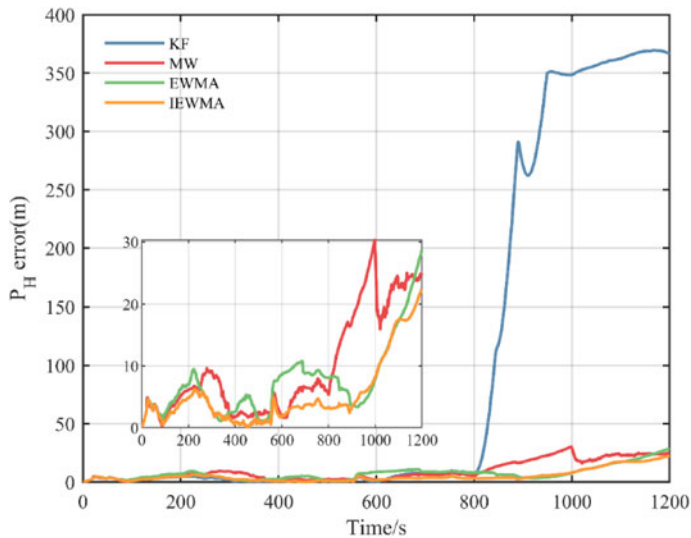**Figure 17.** *Position errors of four methods in land trial.*

Figure 18. *Horizontal position errors of four methods in land trial.*

is obvious that the mean and RMS of horizontal position error for IEWMA are smaller than the others. Therefore, the IEWMA method outperforms the other methods in both navigation accuracy and stability.

As mentioned, the performance of the integrated system depends on the accuracy of R_k. The estimated R_k is shown in Figure 19. It can be seen that R_k of IEWMA is more stable than MW and EWMA at the initial moments (0 s to 600 s). This is because the width of the moving window in MW and the forgetting factor b of EWMA cannot meet the requirements of the environment. Conversely, the adaptive forgetting factor b of IEWMA can decrease to adapt to the stable environment. Additionally, the estimated R_k of IEWMA is the closest to true value, while MW and EWMA are sluggish when noise occurs (800 s to 950 s). When the measurement noise occurs, the forgetting factor of IEWMA becomes smaller, and the weight of the residual in current time increases, which can be sensitive to changes. However, because of the fixed width of the moving window and forgetting factor b, MW and EWMA are still affected by the historical sequence and are too sluggish to estimate the noise accurately.

**Table 5.** *Mean of attitude, velocity and position errors in four methods.*

Method	Attitude (pitch)	Attitude (roll)	Attitude (yaw)	Velocity (E)	Velocity (N)	Velocity (U)	Position (E)	Position (N)	Position (U)
KF	0·02334	0·008384	0·680781	0·490694	0·71575	0·43585	159·2005	37·31923	115·0909
MW	0·003086	0·003837	0·075191	0·046104	0·037349	0·016047	16·42181	14·48248	2·983621
EWMA	0·004551	0·002491	0·058677	0·0322	0·060196	0·045957	8·879652	5·618469	9·074417
IEWMA	0·003026	0·002412	0·089535	0·016455	0·029387	0·007298	8·319802	5·427956	2·037195

Table 6. *RMS of attitude, velocity and position errors in four methods.*

Method	Attitude (pitch)	Attitude (roll)	Attitude (yaw)	Velocity (E)	Velocity (N)	Velocity (U)	Position (E)	Position (N)	Position (U)
KF	0·050807	0·013957	1·300867	1·156426	1·653638	0·875787	321·2462	72·78223	234·7398
MW	0·003424	0·004563	0·078695	0·058616	0·052076	0·022114	27·70016	17·11626	4·160389
EWMA	0·005003	0·003052	0·081959	0·040637	0·081803	0·058244	13·20689	7·145725	13·28029
IEWMA	0·003418	0·003044	0·078417	0·021147	0·044574	0·009189	11·11109	6·773047	2·706211

Table 7. *Mean and RMS of horizontal position errors in four methods.*

	KF	MW	EWMA	IEWMA
Mean	169·1027	24·12699	11·36973	10·39009
Variance	329·3879	32·56171	15·0161	13·01271
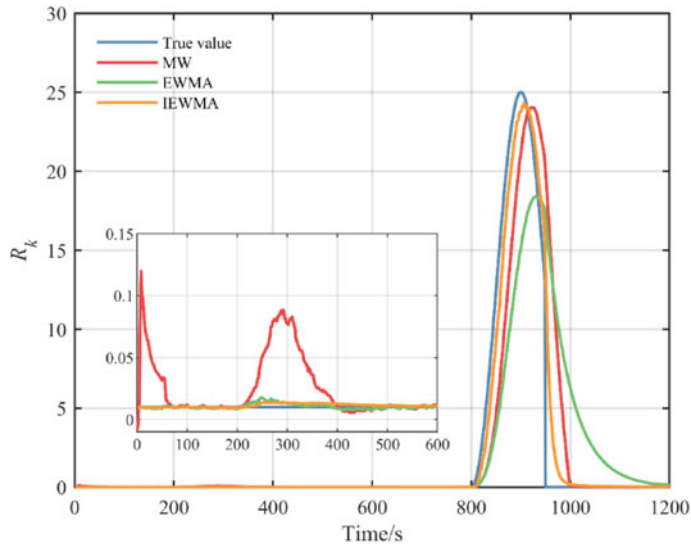
Figure 19. *Diagram of the estimated R_k in land trial.*

5. Conclusions

To eliminate navigation errors introduced by the DVL error in complex underwater environments, an AKF with measurement noise estimator is proposed in this paper. The measurement noise estimator provides accurate noise statistical characteristics for the filter to improve navigation performance. In order to reduce the influence of the historical sequence on the estimated R_k, an adaptive forgetting factor is introduced to the measurement noise estimator for applying to various noise dynamic characteristics. The proposed IEWMA method can be directly utilised in an unknown environment and can adapt to various noise dynamic characteristics. Results of simulation and experience tests show that the AKF based on the measurement noise estimator of the proposed IEWMA method has better performance than MW and EWMA methods in terms of the measurement noise estimation and the navigation accuracy. The navigation results are more stable in low dynamic circumstances and more sensitive in highly dynamic circumstances.

References

Almagbile, A., Wang, J. and Ding, W. (2010). Evaluating the performances of Adaptive Kalman filter methods in GPS/INS integration. *Journal of Global Positioning Systems*, **9**(1), 33–40.

Eliav, R. and Klein, I. (2018). INS/Partial DVL measurements fusion with correlated process and measurement noise. *Proceedings*, **4**(1), 34. https://doi.org/10.3390/ecsa-5-05727.

Franzen, J. and Fingscheidt, T. (2019). Improved Measurement Noise Covariance Estimation for N-channel Feedback Cancellation Based on the Frequency Domain Adaptive Kalman Filter. *ICASSP 2019–2019 IEEE International Conference on Acoustics, Speech and Signal Processing (ICASSP)*, 965–969.

Gao, B., Gao, S., Hu, G., Zhong, Y. and Gu, C. (2017). Maximum likelihood principle and moving horizon estimation based adaptive unscented Kalman filter. *Aerospace Science & Technology*, **73**, 184–196.

Gao, W., Li, J., Zhou, G. and Li, Q. (2015). Adaptive Kalman filtering with recursive noise estimator for integrated SINS/DVL systems. *Journal of Navigation*, **68**(1), 142–161.

González-García, J., Gómez-Espinosa, A., Cuan-Urquizo, E., García-Valdovinos, L. G., Salgado-Jiménez, T. and Cabello, J. A. E. (2020). Autonomous underwater vehicles: localization, navigation, and communication for collaborative missions. *Applied Sciences*, **10**(4), 1256.

Hu, G., Gao, B., Zhong, Y., Ni, L. and Gu, C. (2019). Robust unscented Kalman filtering with measurement error detection for tightly coupled INS/GNSS Integration in hypersonic vehicle navigation. *IEEE Access*, **7**, 151409–151421.

Hu, G., Ni, L., Gao, B., Zhu, X., Wang, W. and Zhong, Y. (2020). Model predictive based unscented Kalman filter for hypersonic vehicle navigation with INS/GNSS integration. *IEEE Access*, **8**, 4814–4823.

Hu, G., Wang, W., Zhong, Y., Gao, B. and Gu, C. (2018). A new direct filtering approach to INS/GNSS integration. *Aerospace Science and Technology*, **77**, 755–764.

Huang, Y. and Zhang, Y. (2017). A new process uncertainty robust Student's *t* based Kalman filter for SINS/GPS integration. *IEEE Access*, **5**, 14391–14404.

Jin, B., Guo, J., He, D. and Guo, W. (2017). Adaptive Kalman filtering based on optimal autoregressive predictive model. *GPS Solutions*, **21**(2), 307–317.

Lee, C.-M., Lee, P.-M., Hong, S.-W., Kim, S.-M. and Seong, W. (2005). Underwater navigation system based on inertial sensor and Doppler velocity log using indirect feedback Kalman filter. *International Journal of Offshore and Polar Engineering*, **15**(2), 8, 88–95.

Liu, K., Zhao, W., Sun, B., Wu, P., Zhu, D. and Zhang, P. (2019). Application of updated Sage–Husa adaptive Kalman filter in the navigation of a translational sprinkler irrigation machine. *Water*, **11**(6), 1269.

Liu, Y., Fan, X., Lv, C., Wu, J., Li, L. and Ding, D. (2018). An innovative information fusion method with adaptive Kalman filter for integrated INS/GPS navigation of autonomous vehicles. *Mechanical Systems and Signal Processing*, **100**, 605–616.

Mohamed, A. H. and Schwarz, K. P. (1999). Adaptive Kalman filtering for INS/GPS. *Journal of Geodesy*, **73**(4), 193–203.

Narasimhappa, M., Mahindrakar, A. D., Guizilini, V. C., Terra, M. H. and Sabat, S. L. (2018). An improved Sage Husa adaptive robust Kalman Filter for de-noising the MEMS IMU drift signal. *2018 Indian Control Conference (ICC)*, 229–234.

Narasimhappa, M., Mahindrakar, A. D., Guizilini, V. C., Terra, M. H. and Sabat, S. L. (2020). MEMS-based IMU drift minimization: Sage Husa adaptive Robust Kalman filtering. *IEEE Sensors Journal*, **20**(1), 250–260.

Narasimhappa, M., Nayak, J., Terra, M. H. and Sabat, S. L. (2016). ARMA model based adaptive unscented fading Kalman filter for reducing drift of fiber optic gyroscope. *Sensors and Actuators A: Physical*, **251**, 42–51.

Raman K. M. (1972). Approaches to adaptive filtering. *IEEE Transactions on Automatic Control*, **17**(5), 693–698.

Sabet, M. T., Mohammadi Daniali, H., Fathi, A. and Alizadeh, E. (2018). A low-cost dead reckoning navigation system for an AUV using a robust AHRS: Design and experimental analysis. *IEEE Journal of Oceanic Engineering*, **43**(4), 927–939.

Sage, A. P. and Husa, G. W. (1969). Algorithms for sequential adaptive estimation of prior statistics. *1969 IEEE Symposium on Adaptive Processes (8th) Decision and Control*, **1969**, 61–61.

Sun, J., Xu, X., Liu, Y., Zhang, T. and Li, Y. (2016). FOG random Drift signal denoising based on the improved AR model and modified Sage-Husa adaptive Kalman filter. *Sensors (Basel)*, **16**(7), 1073.

Tal, A., Klein, I. and Katz, R. (2017). Inertial navigation system/Doppler velocity log (INS/DVL) fusion with partial DVL measurements. *Sensors (Basel)*, **17**, 2.

Wang, J. (1999). Stochastic modeling for real-time kinematic GPS/GLONASS positioning. *Navigation (Washington)*, **46**(4), 297–305.

Xu, Y., Liu, W., Ding, X., Lv, P., Feng, C., He, B. and Yan, T. (2018). USBL Positioning System Based Adaptive Kalman Filter in AUV. *2018 OCEANS-MTS/IEEE Kobe Techno-Oceans(OTO)*. IEEE, 1–4.

Xu, Y., Shen, T., Chen, X.-Y., Bu, L.-L. and Feng, N. (2019). Predictive adaptive Kalman filter and its application to INS/UWB-integrated human localization with missing UWB-based measurements. *International Journal of Automation and Computing*, **16**(5), 604–613.

Yang, C., Shi, W. and Chen, W. (2018). Correlational inference-based adaptive unscented Kalman filter with application in GNSS/IMU-integrated navigation. *GPS Solutions*, **22**(4), 100.

Yang, Y. and Xu, T. (2003). An adaptive Kalman filter based on Sage windowing weights and variance components. *Journal of Navigation*, **56**(2), 231–240.

Yao, Y., Xu, X., Li, Y. and Zhang, T. (2019). A hybrid IMM based INS/DVL integration solution for underwater vehicles. *IEEE Transactions on Vehicular Technology*, **68**(6), 5459–5470.

Yulong, H., Zhang, Y., Wu, Z., Li, N. and Chambers, J. (2018). A novel adaptive Kalman filter with inaccurate process and measurement noise covariance matrices. *IEEE Transactions on Automatic Control*, **63**(2), 594–601.

Zhang, L., Liu, L. and Zhang, L. (2020). Research on position correction method for AUV large depth navigation based on ranging positioning. *Computer Communications*, **150**, 747–756.

Zhang, T., Tang, J., Qin, S. and Wang, X. (2019). Review of navigation and positioning of deep-sea manned submersibles. *Journal of Navigation*, **72**, 1021–1034.